An Efficient Modeling Method of the Ballistic Target for Monostatic/Bistatic Observations

Zaihuan Sun[1], In-O Choi[2], Se-Won Yoon[1], Sang-Bin Cha[3], and Sang-Hong Park[1, *]

Abstract—This paper proposes an efficient method to simulate the micro-Doppler (MD) frequency of a ballistic warhead by considering a real flight scenario in monostatic and bistatic observations. The radar signal is difficult to obtain by changing the observation angle as the conventional electromagnetic software does obtain the reflected signal for a fixed target, so we transformed the pose of the model engaged in micro-motion in a local coordinates, to the pose on the trajectory, by constructing the transformation matrix. Then we obtained the radar signal by using the point scatterer model and high frequency estimation method, physical optics, and compared the MD results by using the short-time Fourier transform. In simulations for various observation scenarios, MD signatures were successfully obtained, and scattering characteristics were accurately analyzed.

1. INTRODUCTION

The goal of ballistic missile defense is to destroy the missiles and their warheads before they can reach their targets. The flight of the ballistic missile is divided into three phases: boost, mid-course, and terminal. Generally, the boost phase is very short and sudden, so detection of the missile at this phase is very difficult. Therefore, the detection and intercept are performed during the mid-course phase when the missile is outside the atmosphere or at a very high altitude [1]. However, a flight of missiles is composed of real warheads and decoys, which have similar shape and similar radar cross section (RCS), so efficient methods to distinguish the warhead from the decoy are required.

Efficient radar techniques for automatic target recognition have been developed; examples include the range profile (RP) [2] and the inverse synthetic aperture radar (ISAR) [3] image. However, because of the similarity of the size and RCS of the warhead and decoy, these methods yield similar results for them and are therefore not appropriate for classifying them. For this reason, the micro-Doppler (MD) effect, which shows the oscillation motion of an object or of any structure component of the object, is widely used. The motion of the warhead generally combines spinning, coning, and nutation motion components, whereas decoys follow a wobbling motion, so an MD image in the time-frequency domain can provide distinct features for the two types of target [4]. However, given the difficulty of the task of obtaining the MD signal of a real ballistic target that is following a ballistic trajectory, the signal should be simulated by using an electromagnetic computation method such as physical optics (PO). However, currently most RCS calculation methods compute RCS by fixing the target while changing the radar line of sight. They cannot effectively provide RCS values of a target that is engaged in micro-motion (MM), especially in bistatic-radar scenarios. Therefore, an efficient method to simulate the RCS data for various flight conditions and observation scenarios is required.

This paper proposes an efficient simulation method to obtain MD of a warhead during flight in a real trajectory under both monostatic and bistatic radar-observation geometries. Using a fixed target engaged in MM in local coordinates, we construct a transformation matrix by using the relationship between the coning axis of the fixed target and the real-time velocity vector on the trajectory. Then we transform the MM of the fixed target to that on the trajectory by using the transform matrix and shift the target to the real-time location. Finally, the radar is placed depending on the observation scenario, and the raw signal for MD is calculated using PO. Comparison of the MD image obtained using this PO model to the short-time Fourier transform (STFT) of the raw data calculated from the point scatter (PS) model demonstrates the efficiency of the proposed method for both monostatic and bistatic scenarios.

2. LIMITATIONS OF EXISTING METHODS, AND PROPOSED METHOD

2.1. Limitation of the Existing Method to Describe Micro-motion

PO is a high-frequency electromagnetic computation method that applies the assumption that the object is much larger than the radar wavelength [5]. Compared with low-frequency methods such as the method of moments, PO is less accurate, but it is very fast, so it is widely used to obtain RPs and ISAR images, which require many complex samples in the frequency domain.

Generally, to obtain the RCS of an object for various frequencies and aspect angles, commercial software changes the line-of-sight (LOS) toward the object and for each LOS, obtains an RCS at radar various frequencies [6]. This method is appropriate for the ISAR image because only simple two-dimensional motion is required. However, MM of a ballistic missile is three-dimensional (3D) and complicated, so merely changing the LOS cannot fully represent MM. Furthermore, in bistatic or multistatic observation geometries, in which the transmitter and receiver are at different locations, the MD image cannot be obtained by varying the LOS. Recently-proposed methods [7, 8] modeled the monostatic/bistatic MD by using the geometric theory of diffraction or physical, but these methods have considered a simple MM; for a given observation scenario, they obtained the signal for MD by changing the LOS, but this method has limited applications to real trajectories. Therefore, a new method is required.

2.2. Proposed Method

2.2.1. Modeling of Warhead And Decoy

MM of a warhead is generally composed of three components: coning, spinning, and nutation (Fig. 1). Nutation motion is a pendulum-like rotation motion in the plane that is formed by the coning and the spinning axes. Nutation is a very small movement, so this paper considers only spinning and coning motions [4, 6].
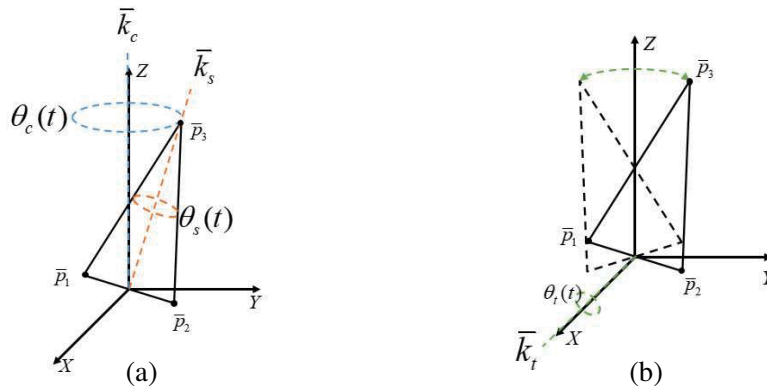

Figure 1. Motion of (a) warhead and (b) decoy. X, Y and Z are local coordinates. The missile is traveling along the Z axis. Variables and processes are described in the text.
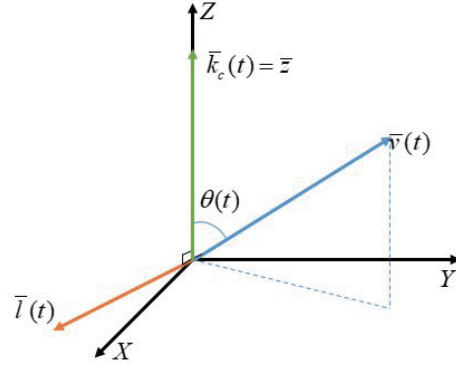
Figure 2. Construction of the transformation matrix.

To model the rotation, we use the Rodrigues rotation matrix formula [9], which is an efficient method to describe the rotation of an object around a rotation axis (Fig. 2). According to this formula, the rotation matrix of a vector $\bar{p}$ around an axis $\bar{k} = (k_x, k_y, k_z)$ by an angle θ is given by

$$\bar{p}(t) = R(t) \cdot \bar{p}, \tag{1}$$

where

$$R(t) = I + [\sin \theta(t)] K + [1 - \cos \theta(t)] K^2, \tag{2}$$

I is the identity matrix, θ the rotation angle, and

$$K = \begin{pmatrix} 0 & -k_z & k_y \\ k_z & 0 & -k_x \\ -k_y & k_x & 0 \end{pmatrix}. \tag{3}$$

Generally, spinning is the rotation around the spinning axis $\bar{k}_s = (k_{sx}, k_{sy}, k_{sz})$ with a rate of spin $\theta_s(t)$, and the spinning rotation matrix $R_s(t)$ can be calculated by formulas (2) and (3) as follows:

$$R_s(t) = I + [\sin \theta_s(t)] K_s + [1 - \cos \theta_s(t)] K_s^2, \tag{4}$$

where I is the identity matrix, θ the rotation angle, and

$$K_s = \begin{pmatrix} 0 & -k_{sz} & k_{sy} \\ k_{sz} & 0 & -k_{sx} \\ -k_{sy} & k_{sx} & 0 \end{pmatrix}. \tag{5}$$

Coning is rotation around a coning axis $\bar{k}_c = (k_{cx}, k_{cy}, k_{cz})$ with the amount of coning $\theta_c(t)$ (Fig. 1(a)), and the spinning rotation matrix $R_c(t)$ can be calculated by formulas (2) and (3) as follows:

$$R_c(t) = I + [\sin \theta_c(t)] K_c + [1 - \cos \theta_c(t)] K_c^2, \tag{6}$$

I is identity matrix, θ the rotation angle, and

$$K_c = \begin{pmatrix} 0 & -k_{cz} & k_{cy} \\ k_{cz} & 0 & -k_{cx} \\ -k_{cy} & k_{cx} & 0 \end{pmatrix}. \tag{7}$$

Then using (1), the warhead motion can be expressed as

$$\bar{p}_{wh}(t) = R_c(t) \cdot R_s(t) \cdot \bar{p} = R_t(t) \cdot \bar{p}, \tag{8}$$

where $R_t(t) = R_c(t) R_s(t)$ is the total rotation matrix. In a similar manner, the micro-motion of the decoy can be expressed.

2.2.2. Real Trajectory Application

The axes of MMs vary along the flight trajectory, so the method introduced in Section 2.2.1 cannot be applied to the real flight trajectory. In this paper, we transform the MM of the target in the fixed local coordinate into that on the trajectory by constructing a transform matrix T_{trj}, then shift the transformed coordinate by using the relative shift between the origin and the position of the target on the trajectory [4].

Assuming that coning axis $\bar{k}_c$ is equal to unit vector $\bar{z}$ of z-axis and that the velocity vector is $\bar{v}(t)$ at time t (Fig. 2), $T_{trj}(t)$ is also calculated by using the Rodrigues rotation formula; contrary to the existing method [4] that uses a rather complicated transformation of two vectors, $T_{trj}(t)$ can be easily obtained by rotating the z axis to $\bar{v}(t)$ by $\theta(t)$ around the axis $\bar{l}(t)$ that is perpendicular to the plane formed by the z axis and $\bar{v}(t)$. $\bar{l}(t)$ is simply obtained by

$$\bar{l}(t) = (l_x(t), l_y(t), \quad l_z(t)) = cross_u(\bar{v}(t), \bar{z}), \tag{9}$$

where $cross_u(\bar{v}(t), \bar{z})$ is the unit vector of the cross-product of $\bar{v}(t)$ and $\bar{z}$. Then T_{trj} is obtained by
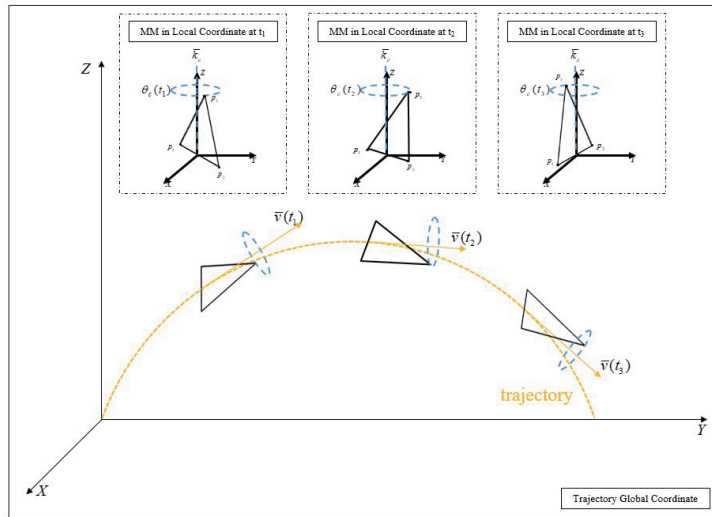
$$T_{Trj}(t) = I + [\sin\theta(t)] K(t) + [1 - \cos\theta(t)] K(t)^2, \tag{10}$$
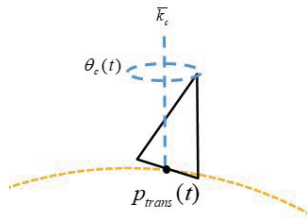
where $K(t)$ is defined as

$$K(t) = \begin{pmatrix} 0 & -l_z(t) & l_y(t) \\ l_z(t) & 0 & -l_x(t) \\ -l_y(t) & l_x(t) & 0 \end{pmatrix}, \tag{11}$$
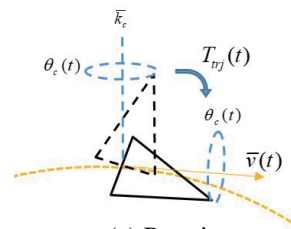
and

$$\theta(t) = \cos^{-1}(\bar{v}(t)^T \bar{z}), \tag{12}$$

(a) Overview

(b) Displacement   (c) Rotation

Figure 3. Transformation of MM of a fixed target to that on the trajectory.

Finally, the coordinate $\bar{p}_{wh}(t)$ or $\bar{p}_{dc}(t)$ of the target in the fixed local coordinate is positioned on the trajectory by transformation using $T_{trj}(t)$, then translation of the transformed vector as

$$\bar{p}_{trj}(t) = T_{trj}(t)\{\bar{p}_{wh}(t) \ or \ \bar{p}_{dc}(t)\} + \bar{p}_{trans}(t) \tag{13}$$

where $\bar{p}_{trans}(t)$ is the relative translation between the origin and the location of the target on the trajectory (Fig. 3).

2.2.3. Overall Procedure

2.2.3.1. Overall Procedure for Signal Processing

The overall procedure to extract MD is composed of six steps (Fig. 4). (1) In the first step, MMs of warhead and decoy are simulated in the local coordinate. In the second step, the flight trajectory is constructed using the ballistic equation [4]. In the third step, the transformation matrix is obtained using (6)–(12), and the target is positioned on the trajectory by using (13). In the fourth step, radars are positioned for each observation scenario, and the radar signal is computed by PO. In the fifth step, RPs are obtained by using the inverse fast Fourier transform (IFFT). However, targets are located at different positions on the trajectory, so the translational motion is removed by using the position of the target on the trajectory (principle explained in Subsection 2.3.2). Finally, the MD image is obtained using STFT of the signal in the range bin of motion-compensated RPs that contain the target.
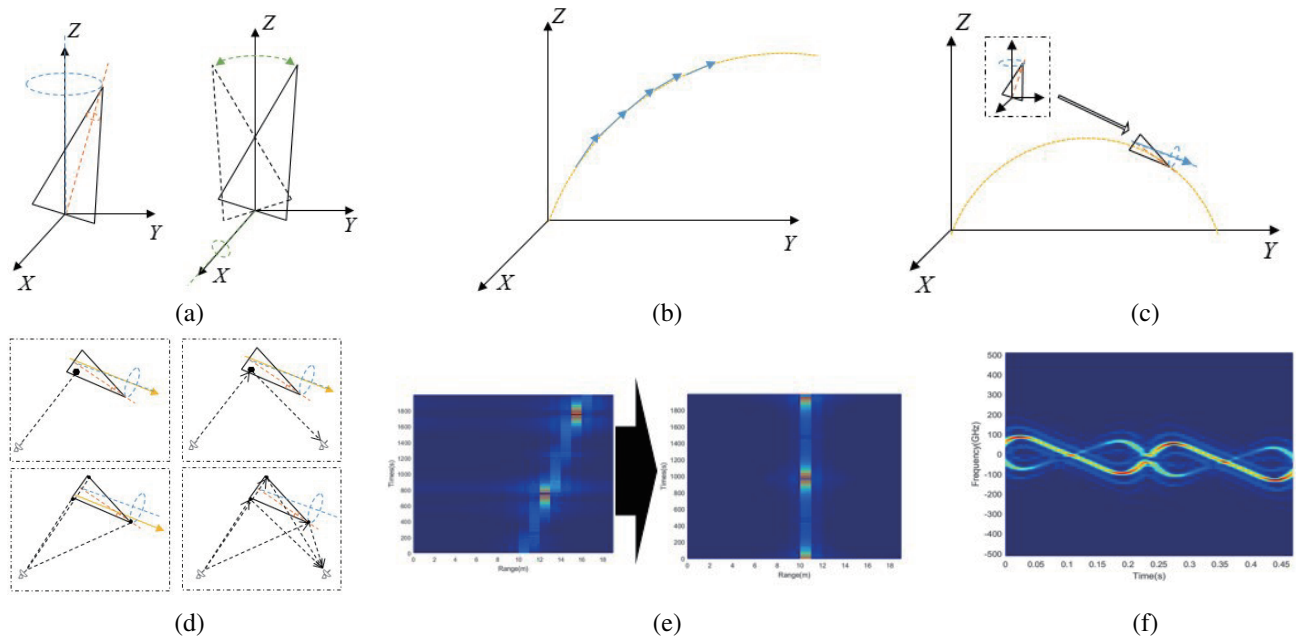

Figure 4. Overall procedure. Process is described in the text. (a) Warhead/decoy in a fixed local coordinate. (b) Construction of flight trajectory to global coordinate. (c) Transformation using the transform matrix. (d) Positioning of radar and RCS computation using PO. (e) IFFT and motion compensation. (f) STFT of the signal in the range bin with the target.

2.2.3.2. Translational Motion Compensation

Even if a target with MM is successfully placed on the trajectory, an MD image cannot be formed, because RPs of the target are located at different positions due to the translational motion. Therefore, the phase error due to the translational motion must be removed. Assuming the received signal for the frequency f at slow-time t' to be $sr(t', f)$, the motion-compensated signal $sr'(t', f)$ is obtained by multiplying $sr(t', f)$ by the conjugate of the phase signal that corresponds to the velocity difference

$dv_t(t')$ of two neighboring RPs along the LOS [10]:

$$s'_r(t', f) = s_r(t', f) \cdot \exp(j4\pi f dv(t')/c),\tag{14}$$

For monostatic radar, $dv(t')$ can be expressed as

$$dv(t') = \left| \frac{\vec{r}(t' + dt') - \vec{r}(t')}{dt'} \right|,\tag{15}$$

where $\vec{r}(t')$ and $\vec{r}(t' + dt')$ are the first and second observed positions after dt', respectively (Fig. 5(a)).
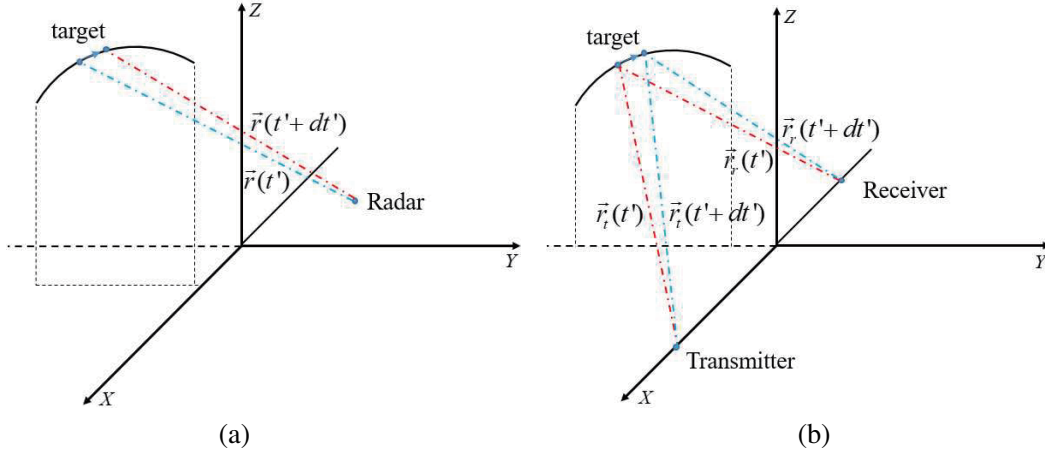

Figure 5. Phase compensation of (a) monostatic and (b) bistatic scenario.

For bistatic radar, the transmitter LOS and receiver LOS have velocity differences $dv_t(t')$ and $dv_r(t')$, respectively:

$$dv_t(t') = \left| \frac{\vec{r}_t(t' + dt') - \vec{r}_t(t')}{dt'} \right|,\tag{16}$$

$$dv_r(t') = \left| \frac{\vec{r}_r(t' + dt') - \vec{r}_r(t')}{dt'} \right|,\tag{17}$$

where $\vec{r}_t(t')$ and $\vec{r}_r(t')$ are respectively the observed distances by the transmitter and receiver at t', and $\vec{r}_t(t' + dt')$ and $\vec{r}_r(t' + dt')$ are those at $(t + dt')$ (Fig. 5(b)).

2.2.4. Analysis of the Difference of Doppler Frequency between Monostatic and Bistatic Radars

Because of the different observation scenarios, MDs of the monostatic and bistatic radars are very different, the difference must be analyzed mathematically. According to (15)–(17), monostatic Doppler frequency f_{Mono} and bistatic Doppler frequency f_{Bi} can be expressed as [12]:

$$f_{Mono} = \frac{1}{\lambda} \cdot dv(t'),\tag{18}$$

$$f_{Bi} = \frac{1}{\lambda} \cdot [dv_t(t') + dv_r(t')],\tag{19}$$

where λ is the radar wavelength.

Assuming that monostatic radar is in halfway along the line from the transmitter to the receiver, with a bistatic angle φ in the bistatic scenario (Fig. 6), f_{Mono} and f_{Bi} are related as [11]:

$$f_{Bi} = \frac{1}{\lambda} \cdot \frac{[dv_t(t') + dv_r(t')]}{2} = \frac{1}{\lambda} \cdot dv(t') \cdot \cos\left(\frac{\phi}{2}\right) = f_{Mono} \cdot \cos\left(\frac{\phi}{2}\right),\tag{20}$$

which shows that the difference of Doppler frequency between bistatic and monostatic depends on ϕ [12]. However, (20) is related to a simple Doppler frequency, so equation must be modified before it can be applied to the observation scenario of MD (analysis provided in Subsection 3.3).
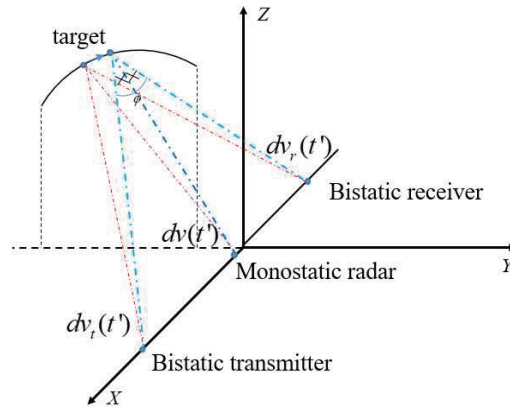
Figure 6. Difference of Doppler frequency between monostatic and bistatic. Variables are described in the text.

3. SIMULATION

3.1. Simulation Condition

The proposed method was applied to a warhead modeled using four isotropic point scatters and to a meshed warhead model (Fig. 7). Both are 3 m in height and 0.5 m in bottom radius. The angular
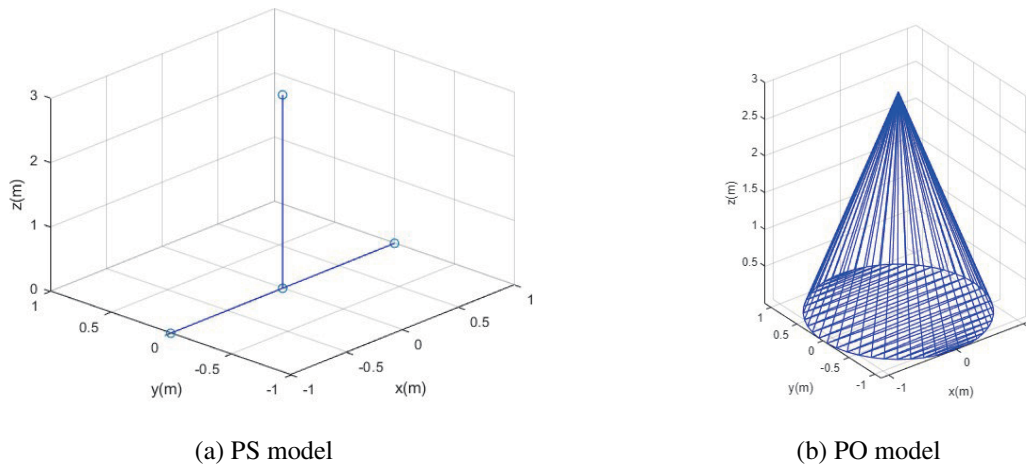

(a) PS model   (b) PO model

Figure 7. Target modeling.

Table 1. Radar parameter.

Parameter	Value
Bandwidth (Hz)	40M
Center frequency (Hz)	10G
PRF (Hz)	4000
Spinning angle speed (rotations/s)	
Coning angle speed (rotations/s)	4
Coning amplitude (°)	15
Time (s)	0.5

velocities of spinning and coning were set to 0 rotation/s and 4 rotations/s, respectively; the spinning angular velocity was set to 0 rad/s because coning motion is generally accompanied by spinning motion. The amplitude of coning motion was set to 15°. Radar parameters were set as bandwidth = 40 MHz (i.e., range resolution 3.75 m) and pulse repetition frequency (PRF) = 4000 Hz to guarantee alias-free sampling of MD. The observation time was set at 0.5 s (Table 1). In modeling the flight trajectory, the trajectory was modeled by applying the parameter of a 500-km range SCUD-C missile to the ballistic equation [13, 14] (Fig. 8). The trajectory is parabolic with a ground length of 500 km and a maximum altitude of 120 km.
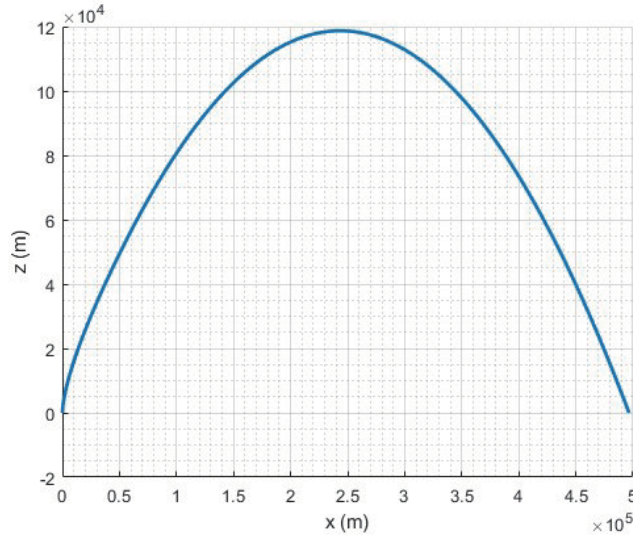

Figure 8. Flight trajectory.

3.2. Comparison of MDs Obtained by Using the PS and PO Models

To demonstrate the accuracy of PO in representing the variation of the scatterer compared with the conventional PS model, the simulation was first conducted using a monostatic scenario. Observation was performed when the warhead reached an altitude = 10 km; to analyze the variation of MD, the radar was set in the same plane as the trajectory, and the LOS was changed with observation angles $1° \leq \delta_m \leq 7°$ (Fig. 9). In measuring the amplitude of MD, a threshold which is 10% of the maximum frequency value was set for each time index, and the minimum $f_{\min}$ and maximum $f_{\max}$ positions of frequency that had frequency larger than the threshold were obtained. Then using the maximum $f_{\min}$ ($\max(f_{\min})$) and minimum $f_{\max}$ ($\min(f_{\max})$) for all time indices, the MD amplitude was calculated as $\min(f_{\max})$-$\max(f_{\min})$.
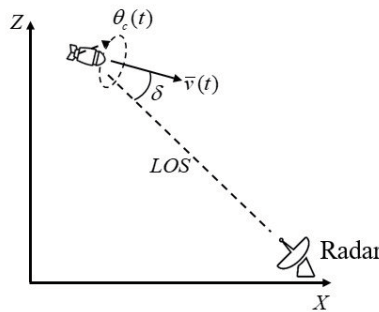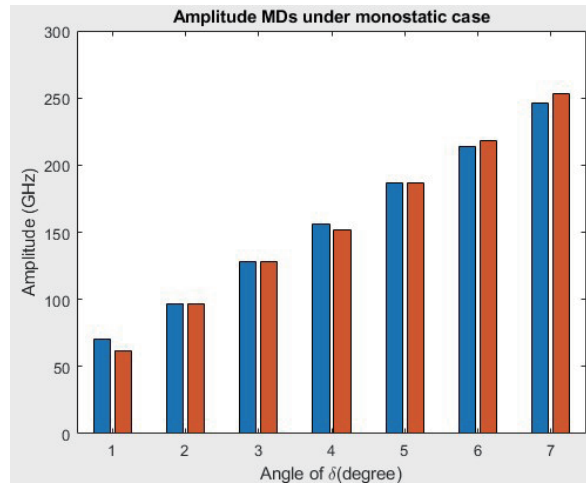

Figure 9. Monostatic scenario.

Figure 10. MD's amplitude comparison with δ_m.

MD of PS model   MD of PO model
(a) $\delta_m = 0°$

MD of PS model   MD of PO model
(b) $\delta_m = 4°$

MD of PS model   MD of PO model
(c) $\delta_m = 7°$

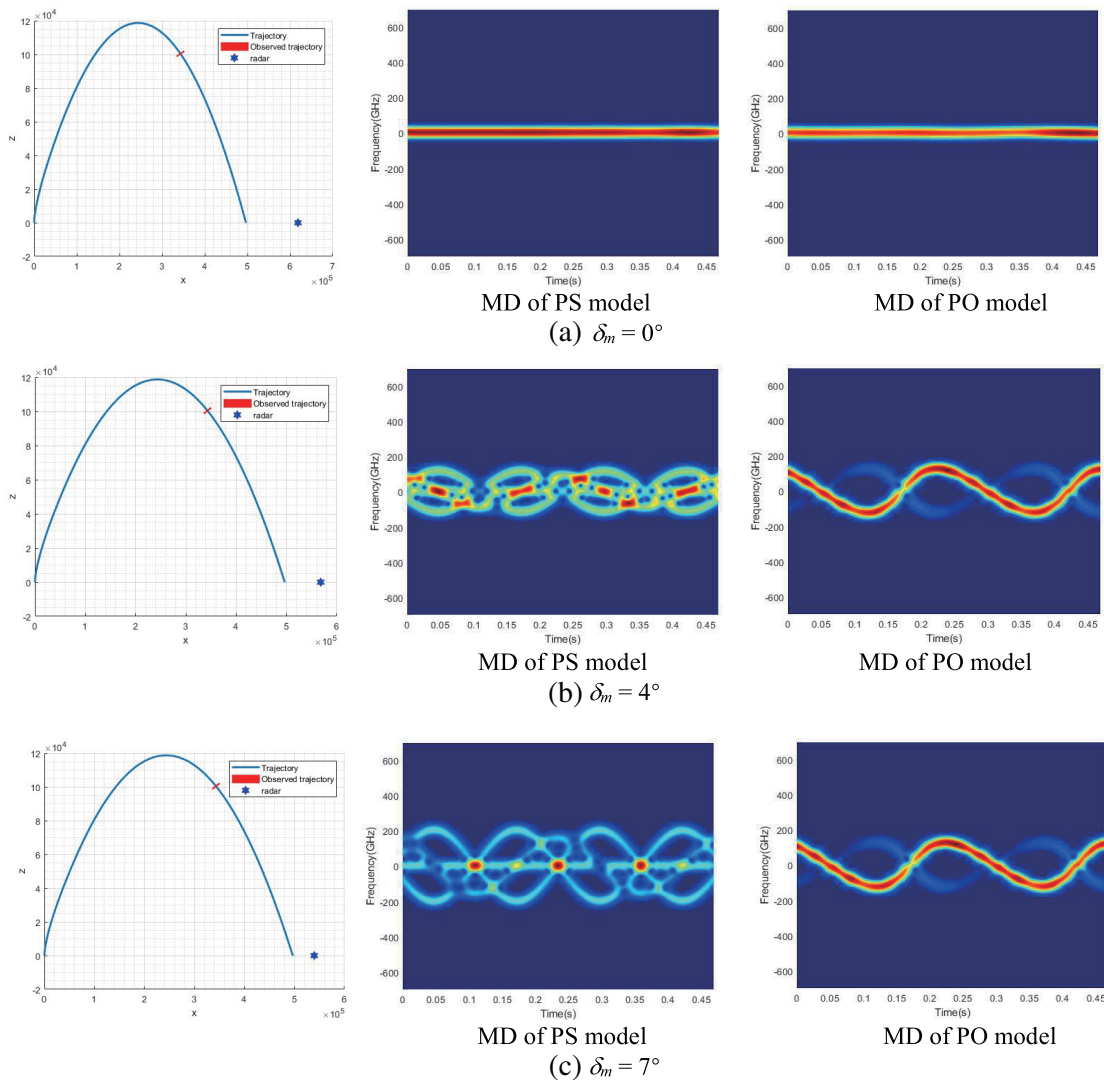**Figure 11.** Comparison of MDs obtained by using PS and PO model.

At $\delta_m = 0°$, the PS and PO models yielded the same result; the direction of the LOS was perpendicular to the plane of MM, so the velocity projected onto the LOS was equal to 0, but the projected velocity was close to 50 Hz due to the resolution of time-frequency image. However, as δ_m was increased, the Doppler frequency increased, and the time-varying nature of MD was represented in the time-frequency domain. The amplitudes of the PS model at 1, 2, 3, 4, 5, 6, and 7° were 70 Hz, 97 Hz, 128 Hz, 156 Hz, 187 Hz, 214 Hz, and 246 Hz, respectively, whereas those of PO model were 62 Hz, 97 Hz, 128 Hz, 152 Hz, 187 Hz, 218 Hz, and 253 Hz (Fig. 10). The two scatterers of the PO model on the bottom tip are the major source of MD, so the amplitudes are very similar to those of PS model; the small difference is due to the error in calculating the threshold. The same MM parameters are used for the two methods, so they calculate similar MD periods.

In addition, to analyze the number and variation of the scatterers, we compared the MD images for $\delta_m = 0°$, 4°, and 7° (Fig. 11). MD is close to 0 at $\delta_m = 0°$, so the scatterers overlapped in a line. As a consequence, the results of the two methods are very similar, and the scatters are observed for the entire observation time. However, for $\delta_m = 4°$ and 7°, the PS model sees the three scatterers for the entire observation time, but PO sees only one scatterer continuously, and the amplitudes of another scatters vary over time. In addition, PO did not see the scatterer that was assumed to exist on the nose tip, because most scattering was contributed by the scatterer on the side tip. This result demonstrates that the PS model is not practical to accurately analyze the MD of the real target even though it is widely used for signal modeling.

3.3. Comparison of MDs Obtained by Monostatic and Bistatic Observation Scenarios

This subsection presents analysis of the difference of MD between monostatic scenario and bistatic scenario. For the monostatic scenario, the result in Fig. 10 was used. However, MD is dependent on the velocity projected to both the transmitter and receiver, and the bistatic angle is a function of the relative motion among the model, transmitter, and receiver, so we simplified the observation scenario by making the MD projected onto the transmitter equal to zero; the transmitter was placed so that the transmitter LOS $= -\bar{u}_{\bar{v}}(t)$, where $\bar{u}_{\bar{v}}(t)$ is the unit vector of $\bar{v}(t)$ which causes $\theta = 0°$ (Fig. 12). Then, the receiver was placed so that bistatic angle δ_r was varied from 1° to 7° with an increment of 1°.
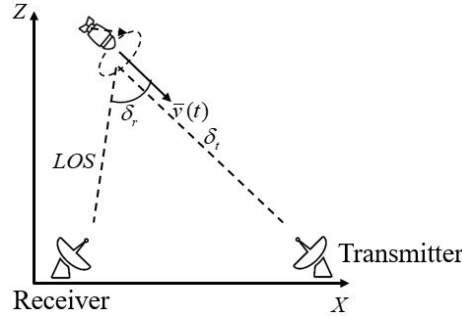

Figure 12. Bistatic scenario.

Analysis was conducted by modifying (19) for the bistatic scenario. MM motion is perpendicular to flight vector (Fig. 14), so the MD $f_{MD,m}$ of MM from monostatic scenario is

$$f_{MD,m} = \frac{1}{\lambda} \cdot v_{MM}(t) \cdot \cos\left(\frac{\pi}{2} - \delta_m\right), \tag{21}$$

and the MD $f_{MD,bi}$ of MM from bistatic scenario is

$$f_{MD,bi} = \frac{1}{\lambda} \cdot \frac{[v_{MM}(t) \cdot \cos(\pi/2 - \delta_t) + v_{MM}(t) \cdot \cos(\pi/2 - \delta_r)]}{2}, \tag{22}$$

where $v_{MM}(t) = r\theta_c(t)$ is the MM rotation velocity, r the MM rotation radius, and $\theta_c(t)$ the coning angular velocity. $\cos\left(\frac{\pi}{2} - \delta_t\right)$ can be eliminated because $\delta_t = 0°$, so $f_{MD,bi}$ can be simplified to $f_{MDBi} = \frac{1}{\lambda} \cdot d\theta(t) \cdot \frac{\cos(\pi/2 - \delta_r)}{2}$. In addition, because $\delta_m = \delta_r$, $f_{MD,bi}$ becomes $f_{MD,mono}/2$. The
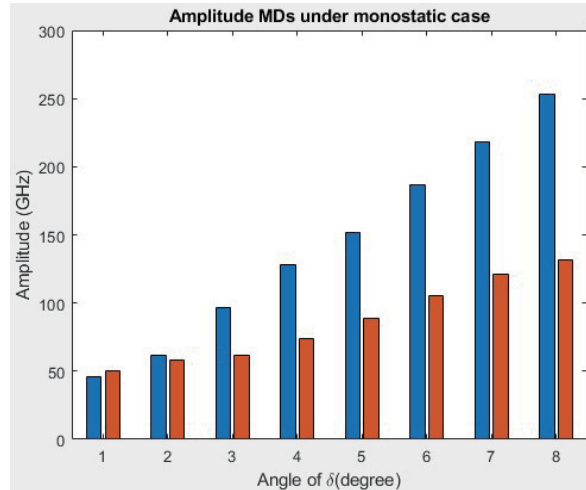
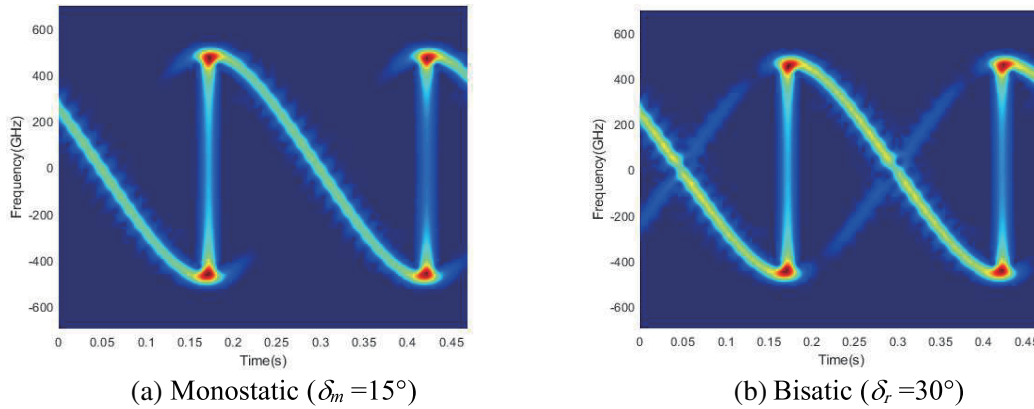**Figure 13.** Comparison of MD amplitude between monostatic and bistatic scenarios.

(a) Monostatic (δ_m =15°)   (b) Bisatic (δ_r =30°)

Figure 14. Comparison of MDs obtained by monostatic and bistatic scenarios ($\delta_m = 15°$ and $\delta_r = 30°$).

simulation result clearly explains the characteristic of bistatic MD (Fig. 13, Fig. 14). For $\delta_m = 1$, 2, 3, 4, 5, 6, and 7°, the amplitudes obtained from the monostatic scenario were 46 Hz, 62 Hz, 97 Hz, 128 Hz, 152 Hz, 187 Hz, 218 Hz, and 253 Hz, respectively, and the amplitudes from bistatic scenario were 50 Hz, 58 Hz, 62 Hz, 74 Hz, 89 Hz, 105 Hz, 121 Hz, and 132 Hz, respectively. In addition, the periods of MD variation for $\delta_m = 15°$ and $\delta_r = 30°$ were exactly equal for the two scenarios, whereas the amplitudes of the scatterers were slightly different (Fig. 14); the scatterer of the bistatic MD is seen for all the observation time even though one scatterer is not visible for $t = 0$–0.15 s and 0.2–0.4 s due to the small scatterer amplitude.

3.4. Comparison with the Measured Data

The proposed method was compared with the measured data acquired by an X-band radar and the micro-motion device introduced in [15] (Fig. 15). The radar system transmitted a chirp signal with a bandwidth = 20 MHz, and the model with a coning angle $\varphi_c = 15°$ was rotated at the angular velocities = 3, 3.75, and 4.25 rad/s and was observed at an aspect angle $\theta_a = 90°$. The measured data was compressed, and the MD image was formed by STFT of the signal in the range bin with the target. Then, the target with the same dimension and MM was modeled, and the MD image was obtained by using the proposed method.

    Comparison with the measurement demonstrates the efficiency of the proposed method (Fig. 16).
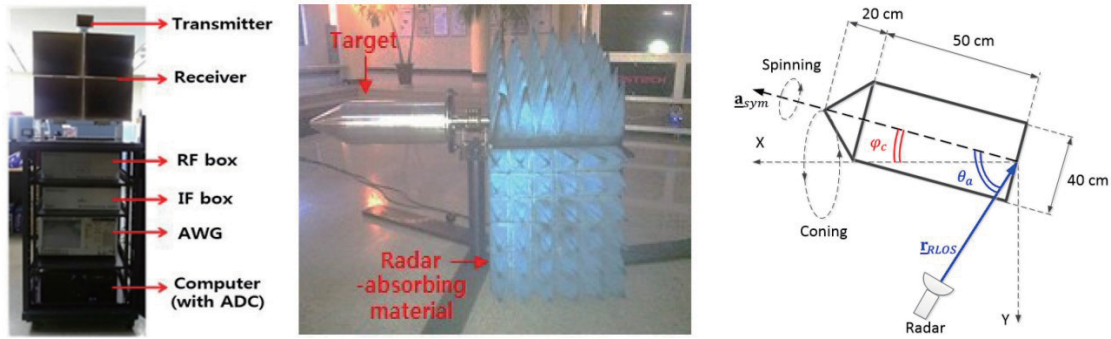
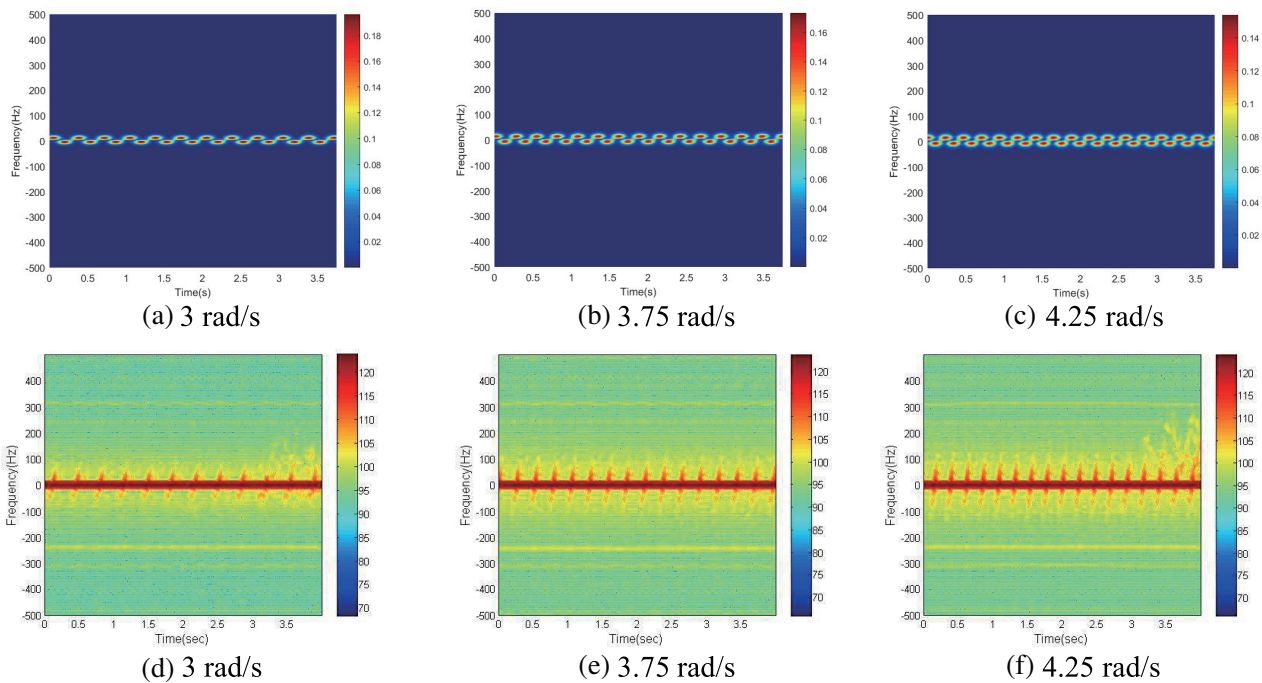**Figure 15.** Measurement system for the ballistic warhead.

Figure 16. Comparison between the simulated and the measured results. MD images (a)–(c) were simulated and those (d)–(f) were measured.

The period and bandwidth of MD are very similar due to the effectiveness of PO. The MD periods of the simulated and measured images are identical and equal to the rotation period of the model. However, the MD bandwidth of the two methods is very different from the Doppler frequency of the nose tip = 322.5 Hz because the reflection from the nose was negligible compared with the body of the target, yielding MD < 100 Hz. Scatterers of the measured and simulated MD images are slightly different. Because PO is based on the approximation by the infinitely large plane boundary, it has a limitation to represent the reflection from the curved surface.

3.5. Application to MM of Wind Turbine

To further verify the possibility of various applications of the proposed method, the proposed method was applied to analyze MM of the wind turbine. For this purpose, a wind turbine composed of three 50-m blades was modeled (Fig. 17(a)). The model was rotated with an angular velocity $\omega_a = 6\pi$ rad/s and observed by a radar with a center frequency = 150 MHz at an aspect angle $\theta_{wt} = 45°$ (Fig. 17(b)); observation at $\theta_{wt} = 90°$ was not conducted because the thickness of the blade was very small. Similar

to the ideal Doppler bandwidth BW given by

$$BW = \frac{2v}{\lambda} * \cos\theta_{wt} = \frac{2\omega_a \times 50}{\lambda} * \cos\theta_{wt} \simeq 667\,\text{Hz}, \tag{23}$$

the bandwidth was very close to $660\,\text{Hz}$ (Fig. 17(c)). In addition, the MD period of each blade $= 0.333\,\text{s/rotation}$ is clearly shown. Therefore, we can conclude that the proposed method can be applied to various cases of MD motion.

(a) Wind turbine model   (b) Observation scenario   (c) MD image
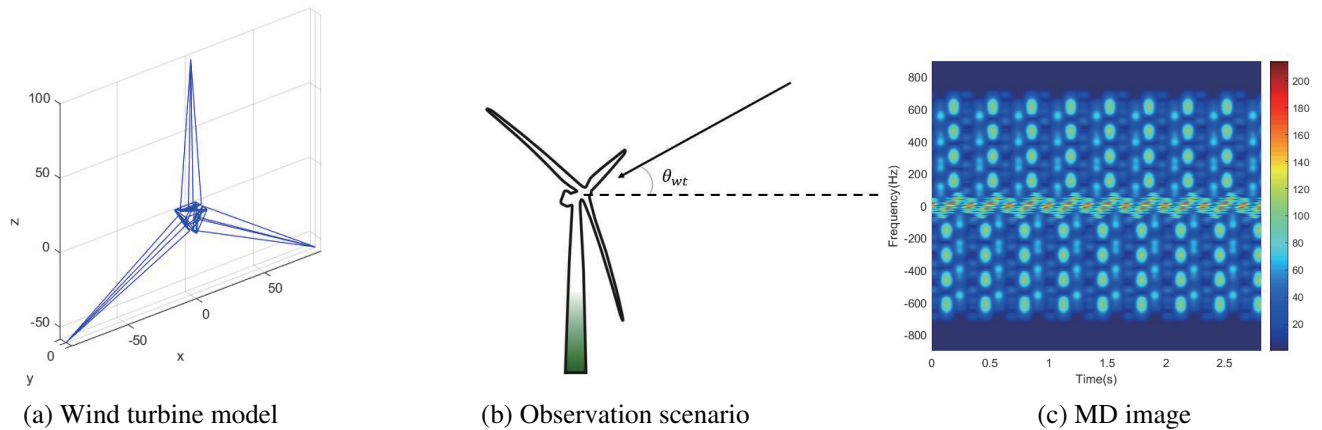
Figure 17. Wind turbine simulation.

4. CONCLUSION

We have proposed an efficient method to simulate MM of the warhead and the decoy on a real flight trajectory. This method simulated a target with real moving status and the radar observation scenarios, whereas previous methods obtained the RCS value by changing only the LOS. To demonstrate the efficiency of the proposed method, we compared PS model and PO model under the monostatic scenario for various LOS angles from $1°$ to $7°$ in increments of $1°$, in which both methods extracted MDs from the MM of target clearly; the scattering nature of the scatterer was better represented by the PO model than by the PS model. Another simulation was performed for the purpose of comparing monostatic and bistatic MDs. In simulations conducted by changing the location of the receiver with MD of the transmitter $= 0$, the characteristic of the scatter in the bistatic scenario was successfully analyzed, and in addition, the dependency of the amplitude of bistatic MD was successfully analyzed. In addition, comparison with the measured data demonstrated the accuracy of the proposed method. The analysis of the MD caused by MM of the wind turbine blade showed that it can be effectively applied to targets with various MMs.

We are currently applying the proposed method to artificial intelligence techniques to classify the warhead and the decoy. The proposed method provides accurate monostatic/bistatic/multistatic MD data for the training database, so we expect to develop a very efficient method that may yield very high classification result by fusing all the available data.

ACKNOWLEDGMENT

REFERENCES

1. Fowler, K. R., "Instrumentation for ballistic missile defense: Lessons learned from the LEAP experiment," *IEEE Transactions on Instrumentation and Measurement*, Vol. 47, No. 5, 1092–1095, Oct. 1998.

2. Atrouz, B., H. Aait Ouazzou, and H. Kimouche, "Features influence on targets classification performance using the high range resolution profiles (HRR profiles)," *2007 IET International Conference on Radar Systems*, 1–4, 2007.

3. Munoz-Ferreras, J. M. and F. Perez-Martinez, "On the doppler spreading effect for the range-instantaneous-doppler technique in inverse synthetic aperture radar imagery," *IEEE Geoscience and Remote Sensing Letters*, Vol. 7, No. 1, 180–184, Jan. 2010.

4. Jung, J.-H., K.-T. Kim, S.-H. Kim, and S.-H. Park, "Micro-Doppler extraction and analysis of the ballistic missile using RDA based on the real flight scenario," *Progress In Electromagnetics Research M*, Vol. 37, 83–93, Jun. 2014.

5. Chatzigeorgiadis, F. and D.Jenn, "A MATLAB physical-optics RCS prediction code," *IEEE Antennas & Propagation Magazine*, Vol. 46, No. 4, 137–139, Aug. 2004.

6. Choi, I.-O., S.-H. Park, K.-B. Kang, K.-T. Kim, "Modeling method of receiving radar signals from warhead and decoy with micro-motion," *The Journal of Korean Institute of Electromagnetic Engineering and Science*, Vol. 30, No. 3, 243–251, 2019.

7. Zou, X.-H., X.-F. Ai, Y.-Z. Li, F. Zhao, and S.-P. Xiao, "Bistatic micro-doppler feature of the precessing cone-shaped warhead," *Journal of Electronics and Information Technology*, Vol. 34, No. 3, 609–615, 2012.

8. Zou, X.-H., X.-F. Ai, Y.-Z. Li, F. Zhao, and S.-P. Xiao. "Bistatic micro-doppler of the spinning warhead with fins," *Journal of Electronics and Information Technology*, Vol. 34, No. 9, 2122–2127, 2012.

9. Johan, E.-M., "Derivation of the Euler-Rodrigues formula for three-dimensional rotations from the general formula for four-dimensional rotations," arXiv General Mathematics, 2007.

10. Cha, S.-B., S.-W. Yon, S.-H. Hwang, M. Kim, J.-H. Jung, J.-H. Lim, and S.-H. Park, "Radar Target Recognition Using a Fusion of Monostatic/Bistatic ISAR Image," *The Journal of Korean Institute of Information Technology*, Vol. 16, 12, 93–100, 2018.

11. Othman, K. A., P. F. S. A. Kamal, N. E. Abd Rashid, and R. S. A. R. Abdullah, "Study of Micro-Doppler effect on target spinning and precession for bistatic radar," *2018 International Conference on Radar, Antenna, Microwave, Electronics, and Telecommunications (ICRAMET)*, 1–4, 2018.

12. Chen, V. C., *The Micro-Doppler Effect in Radar*, Artech House, 2001.

13. Choi, I.-O., S.-H. Kim, J.-H. Jung, K.-T. Kim, and S.-H. Park, "Efficient recognition method for ballistic warheads by the fusion of feature vectors based on flight phase," *The Journal of Korean Institute of Electromagnetic Engineering and Science*, Vol. 30, No. 6, 487–497, 2019.

14. Kim, H.-S., K.-T. Kim, and G.-W. Jeon. "A requirement assessment algorithm for anti-ballistic missile considering ballistic missile's flight characteristics," *Journal of the Korea Institute of Military Science and Technology*, Vol. 14, No. 6, 1009–1017, 2011.

15. Choi, I.-O., K.-T. Kim, J.-H. Jung, S.-H. Kim, and S.-H. Park, "Efficient measurement system to investigate micro-Doppler signature of ballistic missile," *International Journal of Aeronautical Space Sciences*, Vol. 17, No. 4, 614–621, 2016.